

Title:	High Dynamic Rotor Oriented Current Control for Permanent Magnet Synchronous Machines with Saturation Characteristics
Authors:	Tobias Gemassmer, Jan Richter, Mathias Schnarrenberger, Michael Braun
Institute:	Karlsruhe Institute of Technology (KIT) Elektrotechnisches Institut (ETI) Electrical Drives and Power Electronics
Type:	Conference Proceedings
Published at:	PCIM EUROPE 2014 - International Exhibition and Conference for Power Electronics, Intelligent Motion, Renewable Energy and Energy Management Nuremberg, 20-22 May 2014 Publisher: VDE Verlag, Berlin ISBN: 978-3-8007-3603-4 Pages: 153-160
Hyperlinks:	<a href="https://www.vde-verlag.de/proceedings-de/563603016.html">https://www.vde-verlag.de/proceedings-de/563603016.html</a> <a href="http://www.pcim-europe.com">www.pcim-europe.com</a>

# High Dynamic Rotor Oriented Current Control for Permanent Magnet Synchronous Machines with Saturation Characteristics

Tobias Gemaßmer, Karlsruhe Institute of Technology (KIT), Germany, Gemassmer@kit.edu  
 Jan Richter, KIT, Germany, Jan.Richter@kit.edu  
 Mathias Schnarrenberger, KIT, Germany, M.Schnarrenberger@kit.edu  
 Michael Braun, KIT, Germany, Michael.Braun@kit.edu

## Abstract

This paper presents a new approach to adapt classic linear current control design to permanent magnet synchronous machines with saturation characteristics. All needed parameters for the current controller are online calculated from stationary machine measurements. The additional effort compared to control of linear machines is kept as low as possible in order to meet user-oriented requirements. The developed current control scheme is verified by simulation as well as by experimental results.

## 1. Introduction

Rotor oriented current control for permanent magnet synchronous machines (PMSM) with PI-controllers has been well known for several years. However, the design of the controllers in the rotating  $d/q$  reference frame is based on linear machine equations, which are well suited for machines that have negligible saturation characteristics. As soon as the machine becomes highly utilized, saturation effects occur already below the rated current of the machine [1]. In this case classical current controllers with constant parameters show inferior dynamics [2].

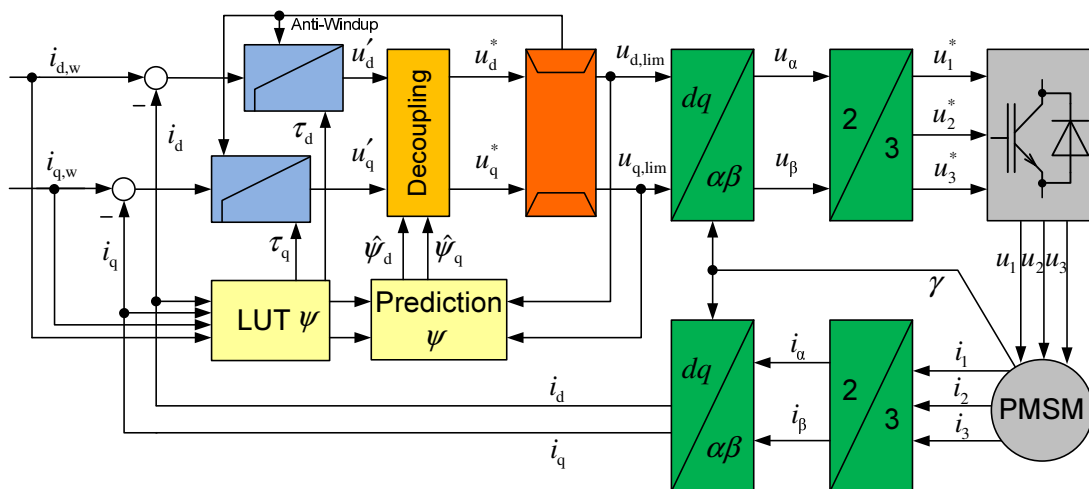


Fig. 1: Rotor oriented current control for PMSM with saturation characteristics.

In this paper a novel approach is presented to adapt classic linear current control design to PMSM with saturation characteristics by extending the conventional rotor oriented control scheme by look-up-tables (LUT) and a prediction of the flux linkage  $\psi$  (see Fig. 1).

## 2. Current control

### 2.1. Machine model

The stator voltage equations of a PMSM in the  $d/q$  reference frame including saturation are [3]:

$$u_d = R_s i_d + L_{dd} \frac{di_d}{dt} + L_{dq} \frac{di_q}{dt} - \omega \psi_q \quad u_q = R_s i_q + L_{qq} \frac{di_q}{dt} + L_{dq} \frac{di_d}{dt} + \omega \psi_d \quad (1)$$

with  $L_{dd}$ ,  $L_{qq}$ ,  $L_{dq}$ ,  $\psi_d$  and  $\psi_q$  depending on the current components  $i_d$  and  $i_q$ . In order to have a rotor oriented current control structure as shown in Fig. 1, the parameters of the controllers have to be adjusted according to the saturating values of the differential inductances  $L_{dd}$  and  $L_{qq}$ . Hence a linearization at the operating point is required.

In the following the parametrization of the current controllers, the decoupling and the limitation of the demanded stator voltage are described, with neglect of the dynamic cross-coupling of the direct and quadrature direction of the machine:  $L_{dq} \approx 0$ .

### 2.2. Parametrization of current controllers

During steady-state operation, the current reference values stay constant. Therefore the values of  $L_{dd}$  and  $L_{qq}$ , which are the slopes of the flux linkages  $\psi_d$  and  $\psi_q$  at the operating point [3], also stay constant. Fig. 2 shows typical characteristic diagrams of the flux linkages  $\psi_{d/q}$  of a highly utilized interior permanent magnet synchronous machine (IPMSM). These relationships between  $\psi_d$ ,  $\psi_q$  and  $i_d$ ,  $i_q$  can be stored in two LUTs.

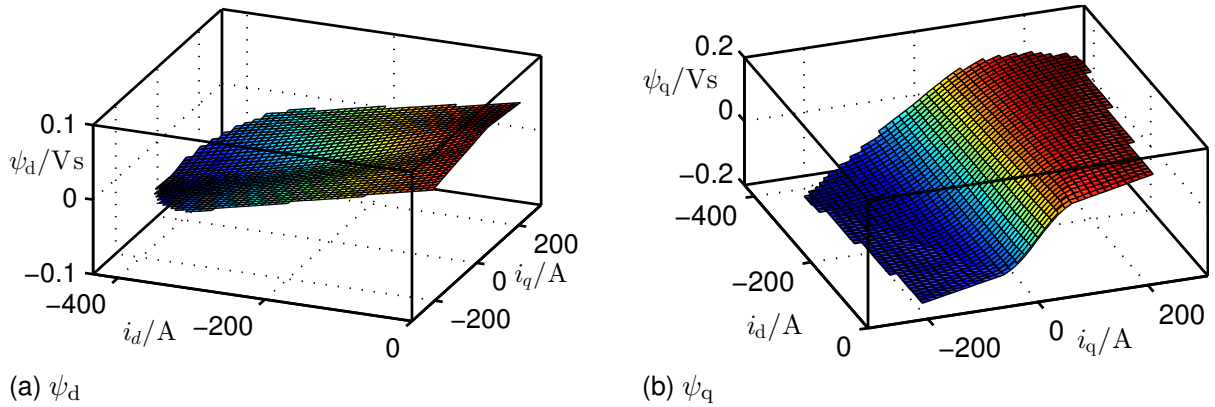


Fig. 2: Flux linkages of an IPMSM for electric vehicles.

As a step in a current reference value  $i_{d,w}$  or  $i_{q,w}$  occurs, the effective inductance  $L_{dd}$  resp.  $L_{qq}$  for that current step has to be identified in order to track the current controller parameters in an appropriate matter. For that purpose, the step response of the current in an inductor with saturation characteristic as shown in Fig. 3 is investigated. Assuming a known differential inductance  $L_{diff}$  for equally spaced values  $\Delta i_n$  of the current and a time period  $T = t_3$ , the total rise of the current within  $T$  can be calculated by:

$$\Delta i_{tot} = u \cdot \left( \frac{t_1}{L_1} + \frac{t_2 - t_1}{L_2} + \frac{t_3 - t_2}{L_3} \right) = u \cdot \frac{t_3}{L_{eff}} \quad (2)$$

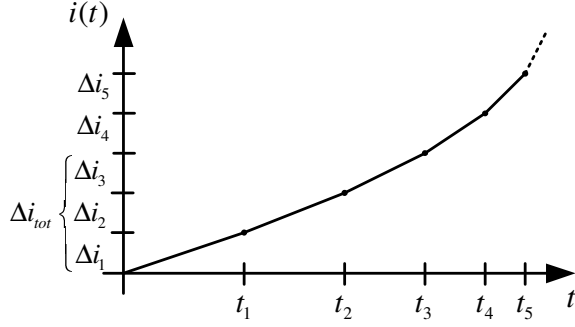


Fig. 3: Current rise in a saturating inductance

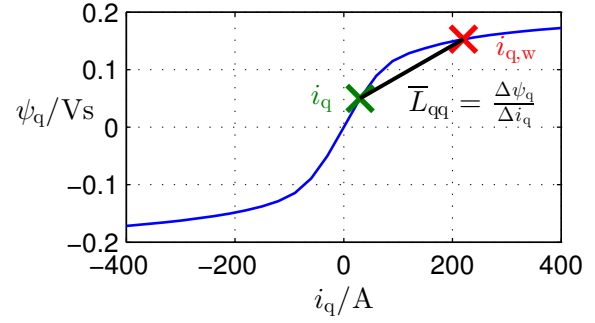


Fig. 4: Inductance  $\bar{L}_{qq}$  during a current step

Applying equally spaced values for  $\Delta i_n$  implies:

$$\frac{\Delta i_{\text{tot}}}{3} = u \cdot \frac{t_1}{L_1} = u \cdot \frac{t_2 - t_1}{L_2} = u \cdot \frac{t_3 - t_2}{L_3} \quad (3)$$

Solving the middle term of (3) for  $\frac{t_1}{L_1}$  and inserting that into the right term results in

$$\frac{t_1}{L_1} = \frac{t_2}{L_1 + L_2} \quad \text{and} \quad \frac{t_2}{L_1 + L_2} = \frac{t_3}{L_1 + L_2 + L_3} \quad (4)$$

With that, the left term of (3) resolves to

$$\Delta i_{\text{tot}} = u \cdot t_3 \cdot \frac{3}{L_1 + L_2 + L_3} = u \cdot \frac{T}{\bar{L}_n} \quad (5)$$

with  $\bar{L}_n$  being the mean value of the occurring inductance values  $L_1$ ,  $L_2$  and  $L_3$ .

According to (5), the required voltage to perform a current step within a time period  $T$  on a saturating inductive device can be calculated using the mean value of the occurring inductance values. The general validity of (5) for  $n = k$  can be proven with the method of mathematical induction and leads to:

$$\Delta i_{\text{tot}} = u \cdot T \cdot \frac{k}{\sum_{n=1}^k L_n} = u \cdot \frac{T}{\bar{L}_n} \quad (6)$$

Assuming very small current steps  $\Delta i_n$  for which the corresponding inductance is known, the value of  $\bar{L}_n$  can be approximated by integration [4]:

$$\bar{L}_n = \frac{1}{k} \sum_{n=1}^k L(i_n) \approx \frac{1}{i_k - i_1} \int_{i_1}^{i_k} L(i) di = \frac{1}{i_k - i_1} \cdot [\psi(i_k) - \psi(i_1)] \quad (7)$$

Hence, the mean value of the inductance for a current step can be taken directly from the flux characteristics. An extra LUT for the differential inductances of the machine is not necessary.

For the parametrization of the two independent current controllers for  $i_d$  and  $i_q$  the inductances in direction of the corresponding current component are needed, therefore the linearization should be done in the appropriate direction. The two differential inductances then are:

$$\bar{L}_{dd} = \frac{\psi_d(i_{d,w}, i_q) - \psi_d(i_d, i_q)}{i_{d,w} - i_d} \quad \bar{L}_{qq} = \frac{\psi_q(i_d, i_{q,w}) - \psi_q(i_d, i_q)}{i_{q,w} - i_q} \quad (8)$$

Fig. 4 illustrates this relation for the quadrature direction of the machine.

With  $\bar{L}_{dd}$  and  $\bar{L}_{qq}$ , the control system time constants  $\tau_d = \frac{\bar{L}_{dd}}{R_s}$  and  $\tau_q = \frac{\bar{L}_{qq}}{R_s}$  for the current step are identified. Now the PI-controllers can be designed with common known design criteria. For a PI-controller with the transfer function

$$G_{PI} = K_P + \frac{K_I}{s} \quad (9)$$

the magnitude optimum method [5] with respect to the dead time  $\tau_\sigma$  of the digital control leads to the parameters

$$K_{P,d} = \frac{\bar{L}_{dd}}{2 \cdot \tau_\sigma} \quad K_{P,q} = \frac{\bar{L}_{qq}}{2 \cdot \tau_\sigma} \quad (10)$$

$$K_{I,d} = \frac{R_s}{2 \cdot \tau_\sigma} \quad K_{I,q} = \frac{R_s}{2 \cdot \tau_\sigma} \quad (11)$$

The resulting structure of the PI-controller including parameter tracking is depicted in Fig. 5 for one current component. The functionality of the anti windup path is described in Section 2.4.

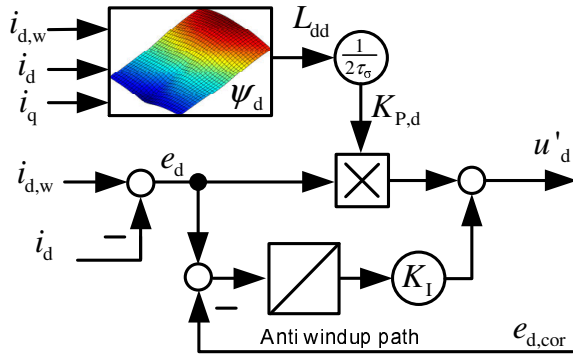


Fig. 5: PI-controller with parameter tracking

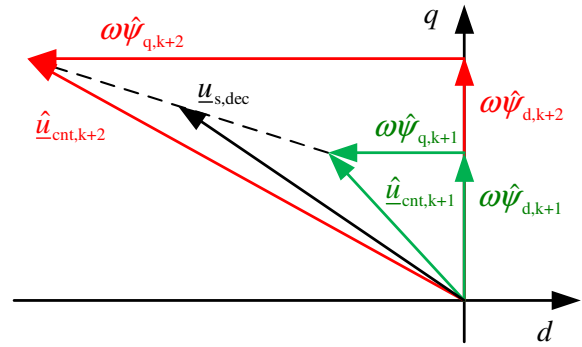


Fig. 6: Decoupling voltage  $\underline{u}_{s,dec}$

### 2.3. Decoupling

According to (1), the decoupling voltages can be obtained directly from the LUTs containing the flux linkages:

$$u_{d,dec} = -\omega \cdot \psi_q(i_d, i_q) \quad u_{q,dec} = \omega \cdot \psi_d(i_d, i_q) \quad (12)$$

These are valid for steady-state operation. As a step of the current reference values occurs, the flux linkage components  $\psi_{d/q}$  change during the subsequent control period. Assuming a linear slope of  $\psi_{d/q}$ , the countervoltages  $u_{d/q,cnt}$  and therefore the decoupling voltage components  $u_{d/q,dec}$  during the pulse period  $T$  are equal to the mean value of the starting point and endpoint of the countervoltage space vector  $\underline{u}_{cnt}$ , as shown in Fig. 6.

Due to the dead time of calculation, the sampled current components always belong to the beginning of the pulse period  $k$ , but not to the pulse period  $k+1$  which the stator voltage  $\underline{u}_{s,k+1}$  is calculated for. Therefore the flux linkages used for decoupling should be predicted from the measured currents and the voltages that were calculated during the last control period:

$$\hat{\psi}_{d,k+1} \approx \psi_d(i_{d,k}, i_{q,k}) + T \cdot [u_{d,k} - R_s \cdot i_{d,k} + \omega \cdot \psi_q(i_{d,k}, i_{q,k})] \quad (13)$$

$$\hat{\psi}_{q,k+1} \approx \psi_q(i_{d,k}, i_{q,k}) + T \cdot [u_{q,k} - R_s \cdot i_{q,k} - \omega \cdot \psi_d(i_{d,k}, i_{q,k})] \quad (14)$$

The flux linkages  $\hat{\psi}_{d/q,k+2}$  at the end of the subsequent control period then can be approximated with use of the voltages  $u'_{d/q,k+1}$  demanded by the current controllers:

$$\hat{\psi}_{d,k+2} = \hat{\psi}_{d,k+1} + T \cdot u'_{d,k+1} \quad \hat{\psi}_{q,k+2} = \hat{\psi}_{q,k+1} + T \cdot u'_{q,k+1} \quad (15)$$

## 2.4. Voltage limitation

During fast transients and at higher speed, the current controllers will demand voltages which cannot be realized by the inverter. In this case, the voltage components need to be limited to reachable values, with the possibly lowest impact on the control performance. This can be achieved by shortening only the dynamic part  $u'_s$  of the demanded voltage space vector  $u_s^*$ , while keeping the value of  $u_{s,OP}$  constant, which is the steady-state voltage at the operating point before the current transition (see Fig. 7a). In this way the phase of  $u'_s$  is maintained and the dynamics of  $i_d$  and  $i_q$  are slowed down in the same rate [6].

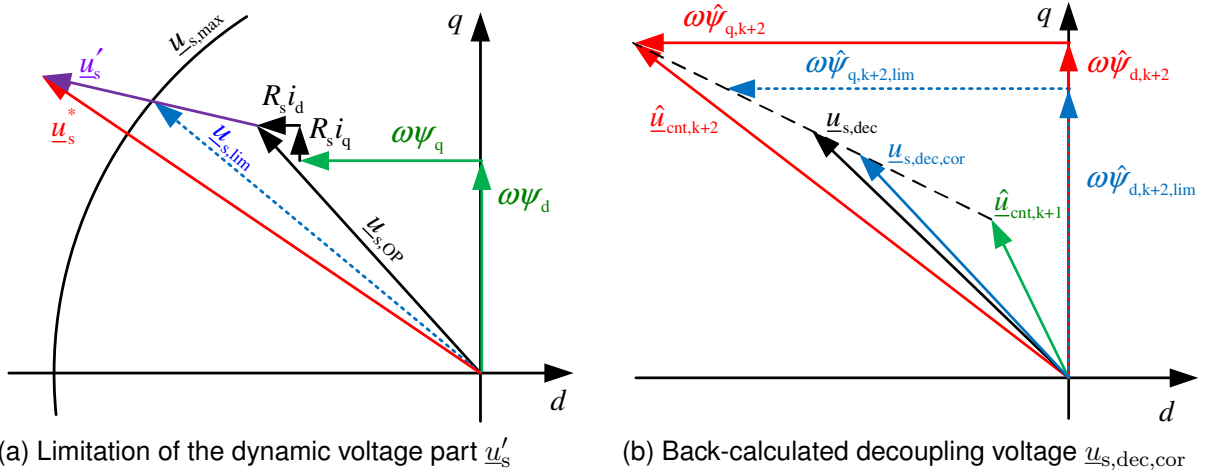


Fig. 7: Vector diagrams of voltage limitation and back-calculated decoupling voltage.

To prevent the integral part of the current controller from wind-up, the shortened voltage  $u_{s,lim}$  is used for back calculation to the current controller. For the back calculation it has to be considered that with a limitation of the controller voltage and a resulting slower rise of the current components, the counter voltage will also not reach the approximated value  $\hat{u}_{cnt,k+2}$  (Fig. 7b). The resulting mean of the countervoltage within the pulse period, which is the decoupling voltage, is smaller and should be also corrected for the purpose of back calculation:

$$u_{d,dec,cor} = \hat{u}_{d,cnt,k+1} + \frac{1}{2} \cdot (\hat{u}_{d,cnt,k+2} - \hat{u}_{d,cnt,k+1}) \cdot \frac{u_{d,lim} - \hat{u}_{d,cnt,k+1}}{u_d^* - \hat{u}_{d,cnt,k+1}} \quad (16)$$

$$u_{q,dec,cor} = \hat{u}_{q,cnt,k+1} + \frac{1}{2} \cdot (\hat{u}_{q,cnt,k+2} - \hat{u}_{q,cnt,k+1}) \cdot \frac{u_{q,lim} - \hat{u}_{q,cnt,k+1}}{u_q^* - \hat{u}_{q,cnt,k+1}} \quad (17)$$

The values of the correction terms  $e_{d/q,cor}$ , which perform the anti windup back calculation (see Fig. 5), then compute to

$$e_{d,cor} = \frac{u_d^* - u_{d,dec} - (u_{d,lim} - u_{d,dec,cor})}{K_{P,d}} \quad (18)$$

$$e_{q,cor} = \frac{u_q^* - u_{q,dec} - (u_{q,lim} - u_{q,dec,cor})}{K_{P,q}} \quad (19)$$

## 2.5. Dead-beat current controller

In order to improve the step and disturbance response of the currents, the PI-controller can be replaced by a dead-beat current control. In this paper, a state controller as being described in [7] has been implemented (see Fig. 8). Tracking of the control parameters in Fig. 8 can be realized identically as for the PI-controller since all parameters also depend on the time constants  $\tau_d$  and  $\tau_q$  of the control paths. Decoupling and voltage limitation have also been accomplished in a similar manner.

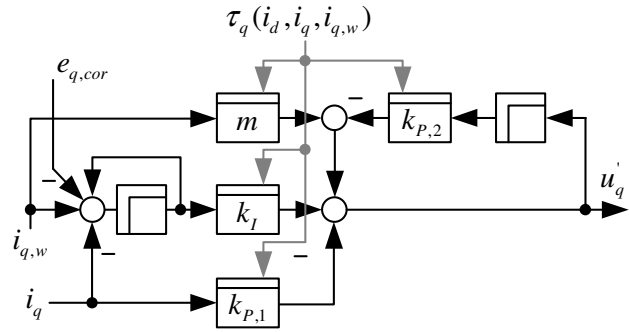


Fig. 8: Dead-beat current controller for one current component.

## 3. Simulation results

Simulations of the proposed control strategy have been carried out in Matlab/Simulink with a machine model as described in [8]. This model is parametrized with the flux linkage characteristics  $\psi_d(i_d, i_q)$ ,  $\psi_q(i_d, i_q)$  shown in Fig. 2 and corresponding differential inductance characteristics  $L_{dd}(i_d, i_q)$ ,  $L_{qq}(i_d, i_q)$  and  $L_{dq}(i_d, i_q)$ , altogether taken from stationary parameter identification of the IPMSM. All parameters are assumed to be independent from temperature and from the rotor position. Further machine parameters can be taken from Tab. 1.

Nominal current	$I_{N,rms}$	121 A	Nominal speed	$n_N$	$4000 \text{ min}^{-1}$
Max. current	$I_{max,rms}$	300 A	Max. speed	$n_{max}$	$11000 \text{ min}^{-1}$
pole pairs	$p$	3	Nominal power	$P_N$	37 kW

Tab. 1: Machine parameters

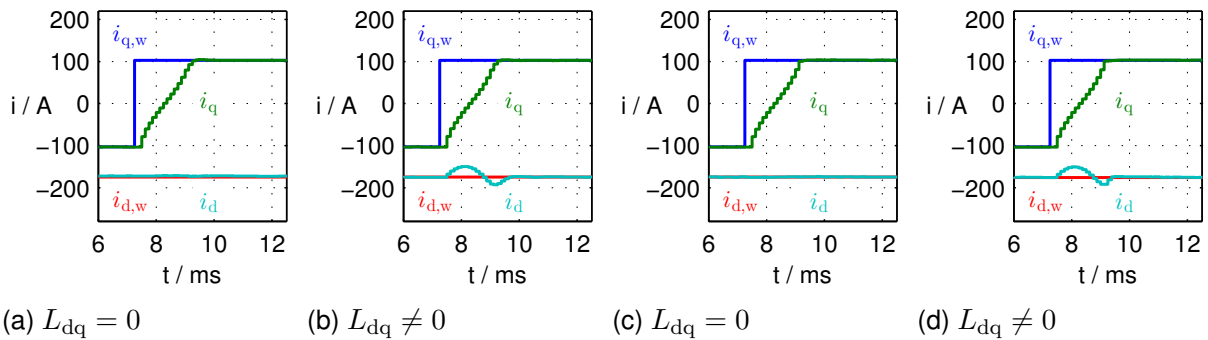


Fig. 9: Simulation results of a torque reversal. (a,b): PI-controller, (c,d): Deadbeat controller

Fig. 9 shows the results of a torque reversal from  $-100 \text{ Nm}$  to  $100 \text{ Nm}$  at a speed of  $1500 \text{ / min}$ . At the torque reversal, the reference value  $i_{q,w}$  changes its sign ( $\pm 103 \text{ A}$ ), while the reference value  $i_{d,w}$  remains constant at  $-176 \text{ A}$ , which are the values for maximum torque per ampere operation for this machine. Fig. 9a and 9c show the torque reversal with  $L_{dq}$  set to 0 in the machine simulation model. The current components are completely decoupled, validating the described scheme of decoupling and back-calculation after voltage limitation. In contrast,

Fig. 9b and 9d show the effects of the dynamic cross-coupling with  $L_{dq} \neq 0$  as in the real machine, letting  $i_d$  slightly deviate during the rise of  $i_q$ . For both cases there is no gain in dynamics by use of the dead-beat controller due to use of the maximum inverter output voltage.

## 4. Experimental results

Verification of the proposed control scheme has been made on a test bench with the IPMSM. Results for different current reference steps at a speed of 1500 / min are depicted in Fig. 10.

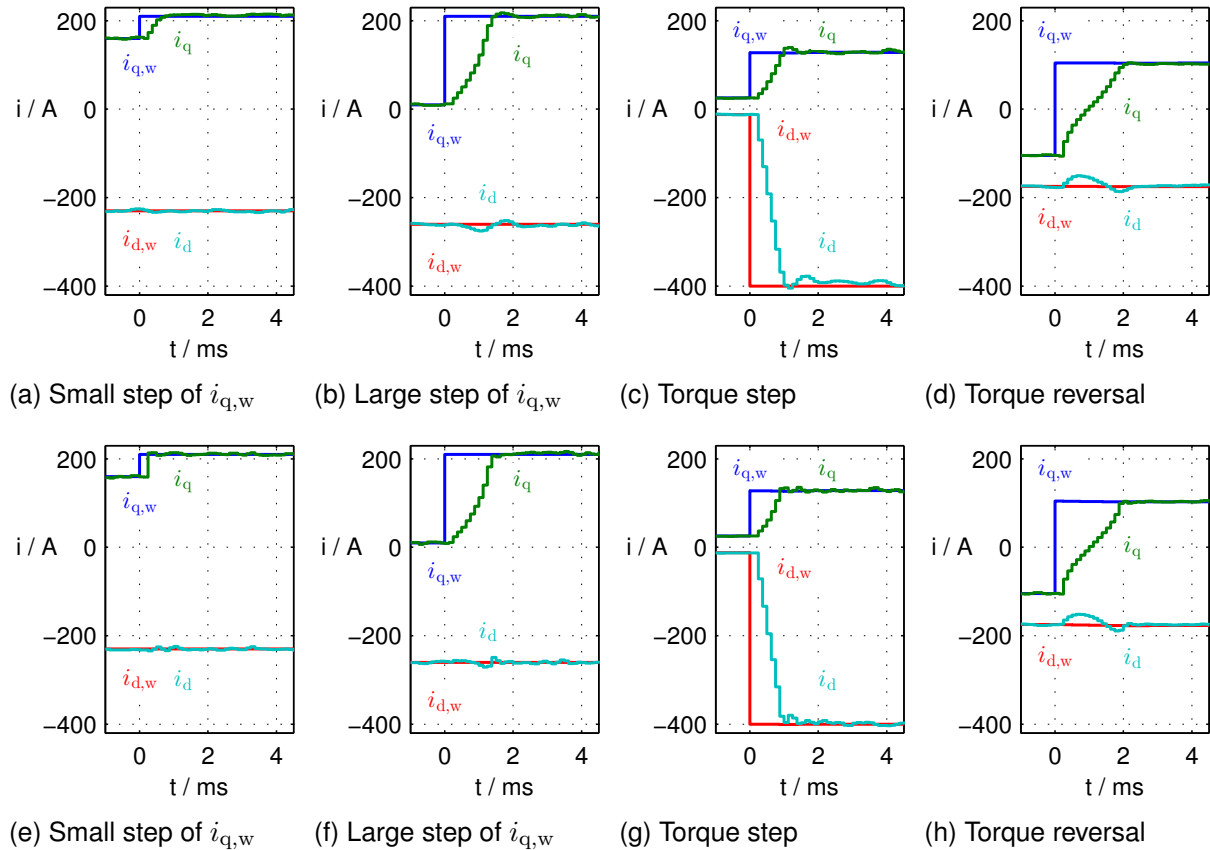


Fig. 10: Current reference steps with PI-controller (a-d) and dead-beat controller (e-h).

Fig. 10a and 10e show a step in the current reference value  $i_q$  which can be realized without reaching the inverter maximum output voltage. The dead-beat controller reaches the reference value within one control period, whereas the PI-controller needs few steps to reach  $i_{q,w}$ . There is no effect on  $i_d$  during the step of  $i_q$  in either case.

A larger step of  $i_{q,w}$  is shown in Fig. 10b and 10f. Both of the controllers work at the voltage limit and therefore there is no higher dynamics by use of the dead-beat controller. The decoupling works satisfactory, the occurring difference of  $i_d$  to its reference  $i_{d,w}$  is corrected faster by use of the dead-beat controller.

Fig. 10c and 10g show a step in the torque reference value from  $T_w = 5 \text{ Nm}$  to 205 Nm, which results in a step of both reference values  $i_{d,w}$  and  $i_{q,w}$ . Again the current step is performed with the maximum voltage of the inverter, so the rise time is the same with both PI- and dead-beat controller.

A torque reversal from  $-100 \text{ Nm}$  to  $100 \text{ Nm}$  is shown in Fig. 10d and 10h. Both PI- and dead-beat controller adjust  $i_q$  within few control periods. However, the influence of the dynamic cross-coupling on  $i_d$  during the reversal can clearly be seen, but has no significant impact on the torque. Comparing simulation and experimental results of the torque reversal, there is no discernible difference in the currents for neither controller, which verifies the simulation model.

Although all performed current steps are located in the nonlinear areas of the flux linkages  $\psi_{d/q}$ , the dynamics as well as the steady-state operation afterwards show very good performances for either current controller, validating all described linearizations and simplifications.

## 5. Conclusion

A way to adapt classic current control schemes to highly utilized PMSM with saturation effects has been proposed. The additional calculation and memory effort has been reduced to a minimum of two flux linkage LUTs for both decoupling and derivation of the time constants. Decoupling and voltage saturation are optimized with regard to both steady state and reference steps. The proposed control scheme has been successfully verified by simulation and experimental results.

## 6. References

- [1] S. Kellner, S. Ebersberger, and B. Piepenbreier. Pmsm d,q-reference frame model using absolute and differential inductance surfaces. In *Power Conversion Intelligent Motion (PCIM Europe)*, pages 953–958, mai 2011.
- [2] J. Weigel and P. Mutschler. Modelling and control of a permanent magnet linear synchronous motor featuring unbalance and saturation including cross-saturation. In *Power Electronics Specialists Conference, 2004. PESC 04. 2004 IEEE 35th Annual*, volume 3, pages 2204–2210 Vol.3, 2004.
- [3] B. Stumberger, G. Stumberger, D. Dolinar, A. Hamler, and M. Trlep. Evaluation of saturation and cross-magnetization effects in interior permanent-magnet synchronous motor. *Industry Applications, IEEE Transactions on*, 39(5):1264 – 1271, sept.-oct. 2003.
- [4] I.N. Bronstein, K.A. Semendjajew, G. Musiol, and H. Mühlig. *Taschenbuch der Mathematik*. Verlag Harri Deutsch, 5 edition, 2001.
- [5] Otto Föllinger. *Regelungstechnik - Einführung in die Methoden und ihre Anwendung*. Hüthig Buch Verlag Heidelberg, 8. auflage edition, 1994.
- [6] Bon-Ho Bae and Seung-Ki Sul. A novel dynamic overmodulation strategy for fast torque control of high-saliency-ratio ac motor. *Industry Applications, IEEE Transactions on*, 41(4):1013–1019, 2005.
- [7] U. Nuß. *Eine allgemeine Methodik zur Modellbildung und Reglersynthese für stromrichtergespeiste Antriebe auf der Basis der zeitdiskreten Zustandsraumdarstellung*. PhD thesis, Universität Karlsruhe, 1994.
- [8] Jan Richter, Patrick Winzer, and Martin Doppelbauer. Application of virtual prototypes of permanent magnet synchronous machines by acausal modeling and simulation. In *ETG Fachbericht*, volume 139, 2013.